Synthesis and Li^+ Intercalation/Extraction in Ultrathin V_2O_5 Layer and Freestanding V_2O_5/Pt/PVA Multilayer Films

Yuanzhi Li, Toyoki Kunitake,* and Yoshitaka Aoki

Frontier Research System (FRS), The Institute of Physical and Chemical Research (RIKEN), Hirosawa 2-1, Wako-shi, Saitama 351-0198, Japan

Received November 2, 2006. Revised Manuscript Received December 3, 2006

A uniform V_2O_5 nanostructured ultrathin film has been prepared by spin-coating followed by heat treatment. This V_2O_5 nanostructured ultrathin film is composed of 4 nm closely connected V_2O_5 domains and has lamellar structure. Compared with a thicker V_2O_5 film (78 nm), the 17 nm V_2O_5 film showed a very good electrochemical performance of fast charge/discharge and excellent electrochemical stability. The excellent electrochemical performance of the V_2O_5 nanostructured ultrathin film is attributed to its nanostructure, which results in short Li^+ diffusion distance and free Li^+ accessibility to intercalation active sites. A facile approach to preparing a freestanding V_2O_5/Pt/PVA multilayer film on a large scale was developed. The thicknesses of the V_2O_5, Pt, and PVA are 22, 57, and 704 nm, respectively. The freestanding multilayer is stable in air, flexible, and robust and exhibits excellent electrochemical performance.

Introduction

Vanadium pentoxide has attracted much attention because of its layered structure that is capable of intercalating Li ions between adjacent layers. Electrical energy is stored in the form of chemical potential upon intercalation and released in the form of electricity upon Li^+ extraction. This interesting electrochemical performance together with its inexpensive and low-toxicity characteristics makes it one of the promising materials for applications in high-energy-density lithium batteries.[1] Unfortunately, the diffusion coefficient of Li^+ in V_2O_5 ($D \approx 1 \times 10^{-12}$ cm^2/s) and the electrical conductivity of V_2O_5 (1×10^{-2} to 1×10^{-3} S/cm) are rather small. Therefore, the Li^+ intercalation is slow, only the surface layer is active in intercalation, and V_2O_5 cannot sustain charge/discharge under a large current density.[2−4] An additional drawback of this electrode is its limited long-term cycling stability, which also restricts its application. Many approaches have been developed to solve these problems and optimize its electrochemical performance. These approaches include choosing different preparation methods,[5,6] optimizing preparation conditions,[7] coating a V_2O_5 thin film on conductive materials,[8,9] doping electrochemically active additives such as TiO_2,[10] Ag,[11] and Cu,[3] and preparing nanostructured V_2O_5 in the form of nanorod,[12] nanotube,[13] hollow microspheres,[14] mesoporous structure,[15] or inverted opal.[16] Among them, nanostructured V_2O_5 materials offer promises to achieve significantly enhanced intercalation capacity and faster intercalation and extraction kinetics because of their large surface-to-volume ratio and a short diffusion distance. Here, we achieved a fast charge/discharge performance and excellent electrochemical stability by designing a nanostructured V_2O_5 ultrathin film and fabricating a freestanding thin V_2O_5/Pt/PVA multilayer film.

Experimental Section

An ITO glass slide (1.9 × 1.2 cm) was put on the rotating stage of a spin coater (Mikasa, Spin Coater 1H-D7). A 100 μL solution of 0.1 mol/L vanadium (V)-tri-*i*-propoxide in a mixed solvent (97.5% ethanol + 2.5% 2-propanol) was dropped on the substrate, and spin-coating was then started at a rotating rate of 4000 r/min

* Corresponding author. Tel: 81-48-467-9601. Fax: 81-48-464-6391. E-mail: kunitake@ruby.ocn.ne.jp.

(1) (a) Park, H. K.; Smryl, W. H.; Ward, M. D. *J. Electrochem. Soc.* **1995**, *142*, 15. (b) Swider-Lyons, K. E.; Love, C. T.; Rolison, D. R. *Solid State Ionics* **2002**, *152−153*, 99.
(2) Lantelme, F.; Mantoux, A.; Groult, H.; Lincot, D. *J. Electrochem. Soc.* **2003**, *150*, A1202.
(3) Coustier, F.; Hill, J.; Owens, B. B.; Passerini, S.; Smyrl, W. H. *J. Electrochem. Soc.* **1999**, *146*, 1355.
(4) Livage, J. *Chem. Mater.* **1991**, *3*, 578.
(5) Zhang, J. G.; Liu, P.; Turner, J. A.; Tracy, C. E.; Benson, D. K. *J. Electrochem. Soc.* **1998**, *145*, 1889.
(6) Julien, J.; Haro-Poniatowski, E.; Camacho-Lopez, M. A.; Es-cobar-Alarcon, L.; Jimenez-Jarquin, J. *Mater. Sci. Eng., B* **1999**, *65*, 170.
(7) Wang, Y.; Shang, H.; Chou, T.; Cao, G. Z. *J. Phys. Chem. B* **2005**, *109*, 11361.
(8) Parent, M. J.; Passerini, S.; Owens, B. B.; Smyrl, W. H. *J. Electrochem. Soc.* **1999**, *146*, 1346.
(9) Kudo, T.; Ikeda, Y.; Watanabe, T.; Hibino, M.; Miyayama, M.; Abe, H.; Kajita, K. *Solid State Ionics* **2002**, *152−153*, 833.
(10) Lee, K.; Cao, G. Z. *J. Phys. Chem. B* **2005**, *109*, 11880.
(11) Chiu, Y. Q.; Qin, Q. Z. *Chem. Mater.* **2002**, *14*, 3152.
(12) a) Sides, C. R.; Martin, C. R. *Adv. Mater.* **2005**, *17*, 125. b) Takahashi, K.; Wang, Y.; Cao, G. Z. *J. Phys. Chem. B* **2005**, *109*, 48.
(13) Nordlinder, S.; Nyholm, L.; Gustafsson, T.; Edstrom, K. *Chem. Mater.* **2006**, *18*, 495.
(14) Cao, A. M.; Hu, J. S.; Liu, H. P.; Wan, L. J. *Angew. Chem., Int. Ed.* **2005**, *44*, 4391.
(15) Liu, P.; Lee, S. H.; Tracy, E.; Yan, Y.; Turner, J. A. *Adv. Mater.* **2002**, *14*, 27.
(16) Sakamoto, J. S.; Dunn, B. *J. Mater. Chem.* **2002**, *12*, 2859.

10.1021/cm0626233 CCC: $37.00
Published on Web 01/12/2007

for 2 min. During this procedure, vanadium (V)-tri-*i*-propoxide was hydrolyzed by air moisture (humidity 70%) to generate a yellow uniform V_2O_5 thin film. To control the thickness of V_2O_5 thin film, we changed the concentration of vanadium (V)-tri-*i*-propoxide from 0.1 to 0.4 mol/L. The V_2O_5 thin film was heated to 250 °C at a rate of 10 °C/min and kept at 250 °C for 3 h in a muffle furnace (KDF-S-70).

Three-hundred microliters of 8 wt % aqueous polyvinyl alcohol was dropped and spin-coated on a glass slide (1.9 × 1.2 cm) at a rotating rate of 3000 r/min for 100 s. The PVA-coated glass slide was then put in the ion-sputtering chamber for Pt coating for 240 s at 6 Pa and 20 mA. Finally, 200 μL of 0.1 mol/L vanadium (V)-tri-*i*-propoxide in the mixed solvent was spin-coated at a rotating rate of 4000 r/min for 120 s. A freestanding multilayer V_2O_5/Pt/PVA thin film was obtained by peeling it off the glass slide. It was fixed by a clip, heated to 150 °C at a rate of 1 °C/min, and dried at 150 °C for 6 h.

Scanning electron microscopy (SEM) images were obtained by using a Hitachi S-5200 scanning electron microscope. X-ray diffraction (XRD) patterns were obtained on a Rigaku Dmax X-ray diffractometer using Cu Kα radiation. Reflectance Fourier transform infrared (FTIR) spectra were taken on a ThermoNicolet Nexus670 spectrometer. ITO glass slides coated with Pt film were used as a reflectance standard as well as a substrate for the V_2O_5 thin film. Electrochemical properties of V_2O_5 thin film were investigated using a standard three-electrode cell, with 1 mol/L $LiClO_4$ solution in propylene carbonate as the electrolyte, a silicon plate coated with Pt film as the counter electrode, and a saturated calomel reference electrode (SCE) as the reference electrode. Cyclic voltammetric (CV) measurements of V_2O_5 thin films were carried out using an electrochemical analyzer (Automatic Polarization System, HZ-3000). The amount of V_2O_5 film was estimated by its area and thickness, and the specific capacities of the V_2O_5 films were obtained by integrating the areas of the $I-V$ curves.

Results and Discussion

Uniform V_2O_5 nanostructured ultrathin film on ITO. Figure 1 presents the morphology of an as-prepared V_2O_5 ultrathin film. The top SEM image of Figure 1a shows that the V_2O_5 thin film is made of rather uniform domains. The corresponding cross-sectional SEM image of Figure 1b shows that the V_2O_5 film has a uniform thickness of 17 nm with a standard deviation of 5%. It can be seen from the TEM image of Figure 1c that the film is composed of V_2O_5 nanoparticles (bright image) of ca. 4 nm. An HRTEM image of Figure 1d further shows that the V_2O_5 nanoparticles have an ordered structure with interplanar spacings of 0.219 nm, although they are surrounded by amorphousV_2O_5. Figure 2a presents an XRD pattern of the V_2O_5 ultrathin film. There are two diffraction peaks that are located at $2\theta = 20.2$ and 41.2°. They may be assigned to the (001) and (002) planes of the orthorhombic structure of V_2O_5,[17] respectively. The corresponding interplanar spacings are calculated to be 0.219 and 0.438 nm, respectively, and match very well to the value measured by HRTEM. No other peaks are observed, and a preferential (001) orientation must exist in the film. This suggests regular stacking of *ab* planes that are built of vanadyl oxygens.[18] This structural feature should be favorable for the intercalation/extraction of Li^+ ions.

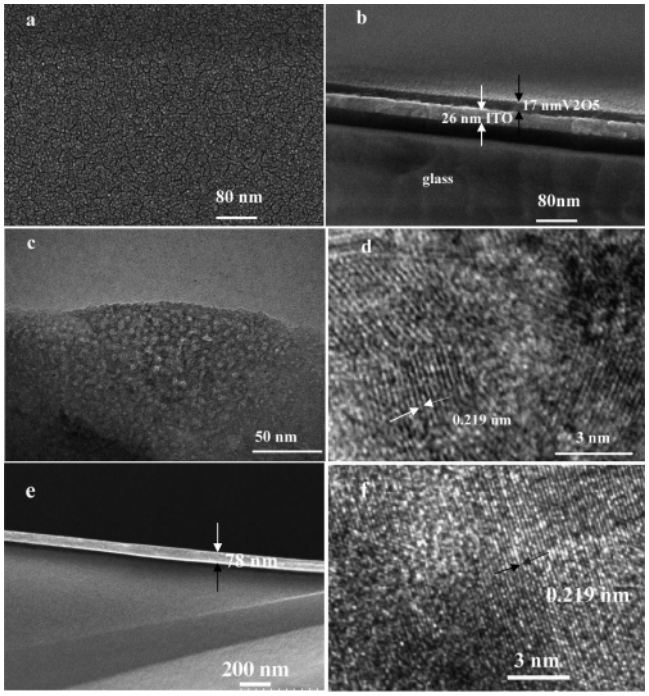

Figure 1. Morphology of the V_2O_5 films: (a) as-prepared 17 nm film, top view (SEM), (b) as-prepared 17 nm film, cross-sectional SEM; (c) as-prepared 17 nm film, TEM; (d) as-prepared 17 nm film, HRTEM; (e) cross-sectional SEM image of the 78 nm V_2O_5 film; (f) HRTEM image of the 17 nm V_2O_5 film after 100 cycles of Li^+ intercalation/extraction (potential range −0.4 to ∼1.0 V).

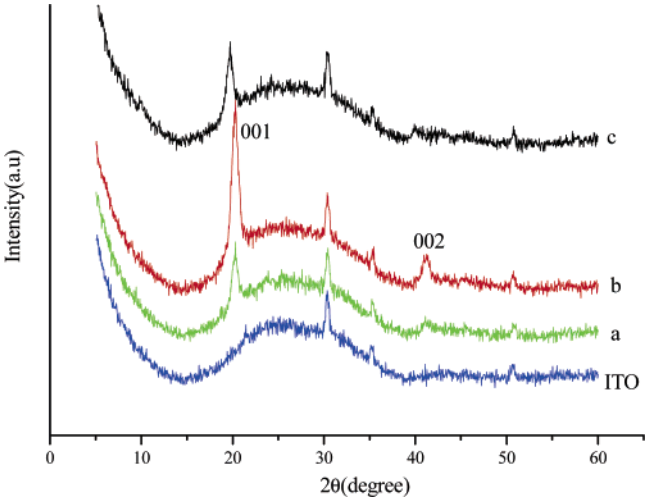

Figure 2. XRD pattern of the 17 nm V_2O_5 film: (a) as-prepared, (b) after 100 cycles of Li^+ intercalation/extraction (potential range −0.4 to ∼1.0 V), (c) after 50 cycles of Li^+ intercalation/extraction (potential range −1.0 to ∼1.0 V).

We separately prepared a thicker V_2O_5 film by using a higher concentration of vanadium (V)-tri-*i*-propoxide (0.4 mol/L) in a mixed solvent. Its top-view morphology is similar to that of the 17 nm V_2O_5 film. The film thickness is estimated to be 78 nm (Figure 1e). The thickness increase (78/17 = 4.6 times) is close to the concentration ratio (4 times) of the precursor solutions. Therefore, the thickness

(17) *Inorganic Crystal Structure Database*, Card 60767; FIZ Karlsruhe: Karlsruhe, Germany, January 1997.

(18) (a) Barreca, D.; Armelao, L.; Caccavale, F.; Noto, V. D.; Gregori, A.; Rizzi, G. A.; Tondello, E. *Chem. Mater.* **2000**, *12*, 98. (b) Audiere, J. P.; Madi, A.; Grenet, J. C. *J. Mater. Sci.* **1982**, *17*, 2973.

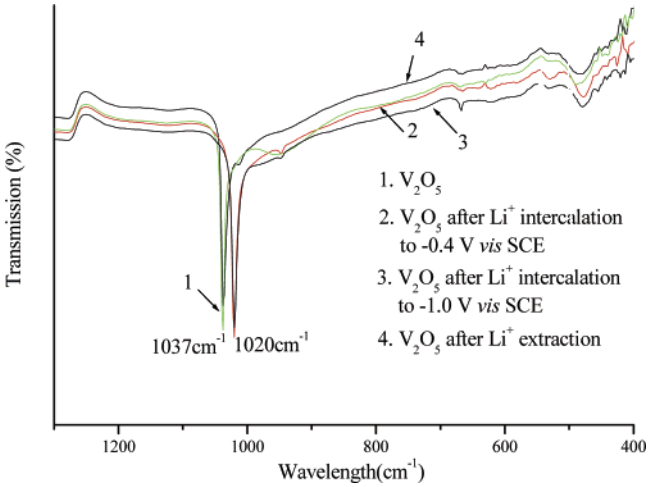

Figure 3. Reflectance infrared spectra of the V_2O_5 ultrathin film.

of V_2O_5 film can be adjusted by changing the precursor concentration.

The electrochemical Li^+ intercalation/extraction process into V_2O_5 can be written as[19,20]

$$Li^+ + xe^- + V_2O_5 = Li_xV_2O_5$$

Li^+ can reversibly intercalate into V_2O_5 in the composition range $0 < x \leq 2$, with the working potential decreasing from 3.5 to 2.0 V vs Li^+/ Li. For larger Li contents, the electrochemical Li^+ intercalation below 1.9 V vs Li has been reported to lead irreversibly to formation of ω phase.[21] In the case of our film, the specific capacity of V_2O_5 is 138 mA h per g of V_2O_5 at a scan range of 1.0 to about −0.4 V vs SCE, corresponding to $Li_{0.93}V_2O_5$. Increasing the potential range to 1.0 to about −1 V vs SCE results in enhancement of the specific capacity to 262 mA h per g of V_2O_5, corresponding to $Li_{1.78}V_2O_5$. It is clear that the specific capacity of V_2O_5 depends on the intercalation depth of Li^+.

The structural change of the V_2O_5 ultathin film that takes place in conjunction with Li^+ intercalation/extraction was examined by FTIR, XRD, and HRTEM characterizations. Figure 3 shows reflectance infrared spectra of the 17 nm V_2O_5 film. The as-prepared V_2O_5 ultrathin film shows a sharp strong absorption at 1037 cm^{-1}, which is assigned to the stretching vibration of the vanadyl bond (V═O).[21] After Li^+ intercalation to the potential of −0.4 V, this band shifts to a lower wavelength number (1020 cm^{-1}), but its intensity remained almost unchanged. This shift is attributed to the presence of a V^{4+}−O group or the existence of a Li^+−O−V bond upon Li^+ interaction.[22b] The FTIR spectra remained unchanged after additional Li^+ intercalation to the potential range of −1.0 V. The reflectance infrared spectrum was essentially reverted to that of the fresh V_2O_5 ultrathin film after Li^+ extraction. These observations indicate that the

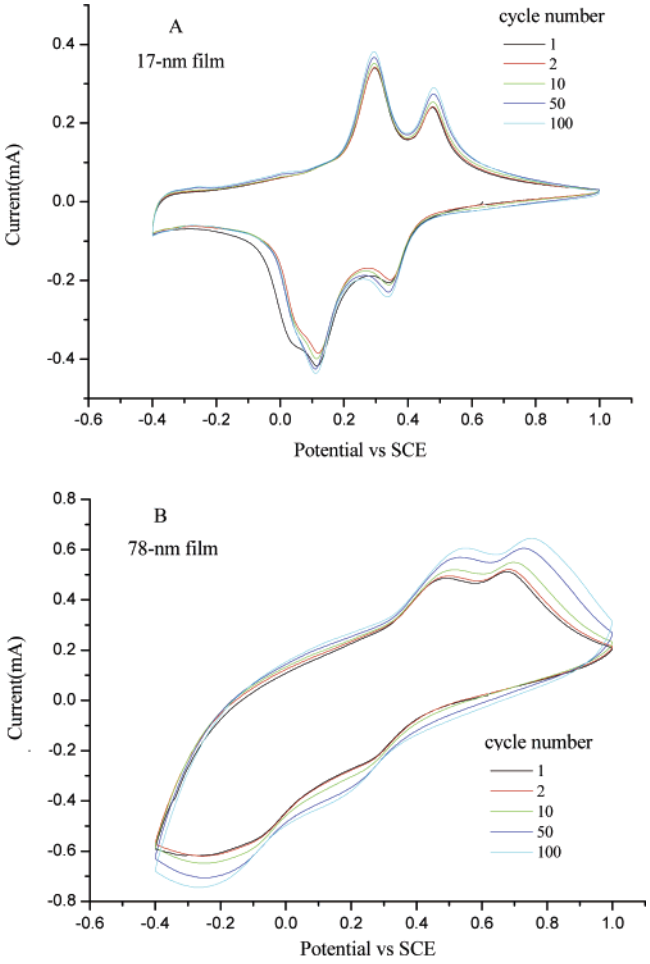

Figure 4. Cyclic voltammograms of the (A) 17 nm V_2O_5 film and the (B) 78 nm film using a scan rate of 50 mV/s.

structure of the V_2O_5 ultrathin film remains intact after cycles of Li^+ intercalation and extraction.

The FTIR data were supported by XRD results, as shown in Figure 2b. After 100 cycles of Li^+ intercalation/extraction (potential range −0.4 to ∼1.0 V), the XRD peak positions remain unchanged from those of the as-prepared film, but the XRD peaks were intensified. Apparently, the layered structure of V_2O_5 remained unchanged, but its crystallinity was improved after interaction/extraction cycles. These results are consistent with the HRTEM observation (Figure 1f). Li^+ intercalation/extraction cycle (potential range −0.4 to ∼1.0 V) induced the crystallization of the surrounding amorphous V_2O_5 of V_2O_5 nanoparticles, but the interplanar spacings of V_2O_5 nanoparticles remained unchanged. Increasing the potential range of Li^+ intercalation/extraction from 1.0 to about −0.4 V vs SCE to 1.0 to about −1.0 V vs SCE leads to the structural change of the V_2O_5 ultrathin film characterized by an increase in the lattice distance from 0.219 to 0.225 nm (measured by XRD). The possible reason is that a small amount of Li^+ ion exists in the layered structure of the V_2O_5 ultrathin film after experiencing the Li^+ intercalation/extraction.

Figure 4A shows typical cyclic voltammograms of the 17 nm film using a scan rate of 50 mV/s. Two well-defined cathodic reduction peaks are found at 0.11 and 0.34 V that are attributed to Li^+ intercalation. The well-defined anodic peaks at 0.29 and 0.48 V correspond to Li^+ extraction. The

(19) Whittingham, M. S. *Chem. Rev.* **2004**, *104*, 4271.
(20) a) Leger, C.; Bach, S.; Soudan, P.; Pereira-Ramos, J. P. *J. Electrochem. Soc.* **2005**, *152*, A236. (b) Mantoux, A.; Groult, H.; Balnois, E.; Doppelt, P.; Gueroudji, L. *J. Electrochem. Soc.* **2004**, *151*, A368.
(21) a) Pinna, N.; Willinger, M.; Weiss, K.; Urban, J.; Schlogl, R. *Nano Lett.* **2003**, *3*, 1131. (b) Surca, A.; Orel, B.; Drazic, G.; Pihlar, B. *J. Electrochem. Soc.* **1999**, *146*, 232.
(22) Sugimoto, W.; Iwata, H.; Yasunaga, Y.; Murakami, Y.; Takasu, Y. *Angew. Chem., Int. Ed.* **2003**, *42*, 4092.

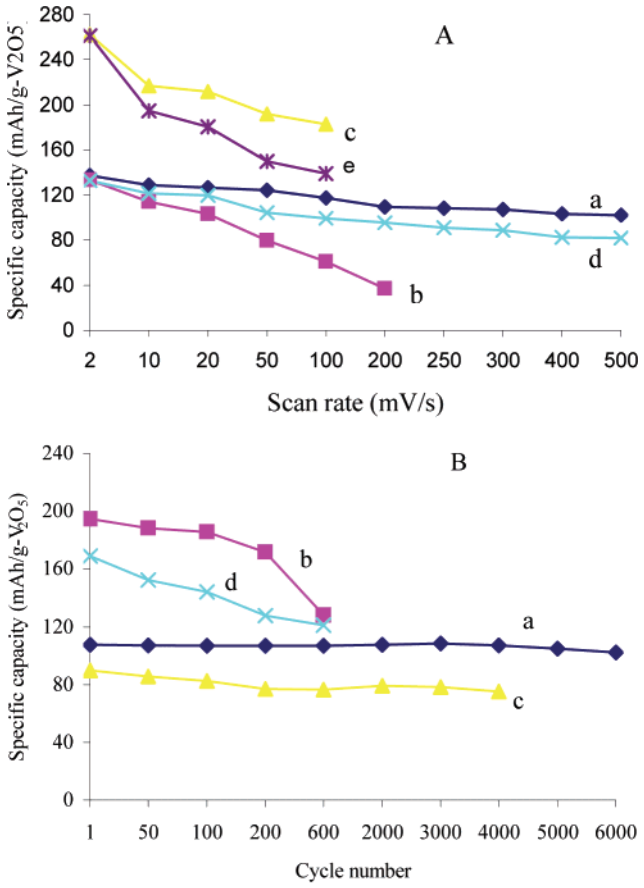

Figure 5. (A) Specific capacity of the V_2O_5 films as a function of scan rate in the first scan cycle: (a) 17 nm film, potential range 1.0 to −0.4 V vs SCE; (b) 78 nm film, potential range 1.0 to about −0.4 V vs SCE; (c) 17 nm film, potential range 1.0 to about −1.0 V vs SCE; (d) V_2O_5/Pt/PVA multilayer, 1.0 to about −0.4 V vs SCE; (e) V_2O_5/Pt/PVA multilayer, 1.0 to about −1.0 V vs SCE. (B) Specific capacity of the V_2O_5 films as a function of cycle number: (a) 17 nm film, 1.0 to about −0.4 V vs SCE, 250 mV/s; (b) 17 nm film, 1.0 to about −1.0 V vs SCE, 50 mV/s; (c) V_2O_5/Pt/PVA multilayer, 1.0 to about −0.4 V vs SCE, 250 mV/s; (d) V_2O_5/Pt/PVA multilayer, 1.0 V to about −1.0 V vs SCE, 30 mV/s.

presence of the symmetric peak groups reveals that intercalation and extraction of Li^+ is highly reversible. Figure 4B gives cyclic voltammograms of the 78 nm film at the same scan rate (50 mV/s). At this scan rate, 42% of the 78 nm film remains inactive, but almost all of the 17 nm film (91%) is active. In contrast to the 17 nm film, the thicker film exhibits less distinctive cathodic and anodic peaks. The intercalation and extraction potentials shift by 0.36 V to a lower position and by 0.21 V to a higher position, respectively, relative to those of the 17 nm film. The electrochemical behavior of these two films is contrasting. The 17 nm film shows a distinctive reversibility of Li^+ incorporation, but the 78 nm film gives slowly changing behavior upon repeated scan cycles. It is clear that intercalation and extraction of Li^+ proceeds essentially reproducibly during repeated potential scan (100 times) in the case of the ultrathin film matrix.

The kinetic process of Li^+ incorporation is further affected by scan rate and scan range. Figure 5A shows the specific capacities of the 17 and 78 nm films as function of scan rate. The former film has a specific capacity of 138 mA h g^{-1} at a low scan rate of 2 mV/s (Figure 5A, curve a). This capacity is comparable to the theoretical capacity (130 mA h g^{-1}) of $LiCoO_2$ used as cathode material in commercial lithium rechargeable battery.[20] The specific capacity decreases slightly with increasing scan rate to 74% of the original value at a very high scan rate of 500 mV/s. In contrast, the specific capacity of the 78 nm film decreases more sharply with increasing scan rates, despite its specific capacity being virtually identical to that of the 17 nm film at the low scan rate of 2 mV/s (Figure 5A, curve b). Clearly, Li^+ migration in and out of the V_2O_5 film occurs to a similar extent at the lowest scan rate of 2 mV/s. As the scan rate is enhanced, Li^+-ion migration becomes incapable of following the speed of the potential change. This time lag is greater with the thicker film, and 73% of the 78 nm V_2O_5 remains inactive at the scan rate of 200 mV/s.

When the potential range was increased to 1.0 to about −1 V vs SCE (formation of $Li_{1.78}V_2O_5$), the specific capacity of the 17 nm film increases from 138 mA h per g of V_2O_5 (1.0 to about −0.4 V) to 262 mA h per g of V_2O_5 at 2 mV/s (Figure 5A, curve c). The scan-rate dependence is rather large in this case, and 70% of the capacity at 2 mV/s is reserved at the scan rate of 100 mV/s. The larger scan-rate dependence is attributed to the decrease in the diffusion coefficient of Li^+ ions with increasing intercalation depth of Li^+.[21] The capacity loss after 600 consecutive cycles is 20% (Figure 5B).

One of the advantages of ultrathin V_2O_5 films is high efficiency and reversibility of migration of Li^+ ions within the film. Highly efficient Li^+ migration is apparent from a lessened sensitivity of the specific capacity to enhanced scan rates (Figure 5A, curve a). In addition, satisfactory reversibility was confirmed by using the 17 nm film. Figure 5B shows specific capacity of the V_2O_5 films as a function of cycle number. The film was tested at the very high charge/discharge rate of 250 mV/s, at which it has 79% of the capacity measured at a low scan rate of 2 mV/s. Well-defined cathodic and anodic peaks are kept essentially unchanged even after 6000 cycles. The final loss of the specific capacity is only 5% (Figure 5B, curve a), suggesting the excellent electrochemical stability and high cycling fatigue resistance of the V_2O_5 ultrathin film. Thus, the V_2O_5 ultrathin film shows excellent performances of fast intercalation/extraction and very good cycling stability, which are comparable to RuO_2, an expensive supercapacitor electrode.[22]

Freestanding V_2O_5/Pt/PVA Multilayer Film. The effective capacity of V_2O_5 in practical applications will be enhanced when thicknesses of the electrode and supporting layer are reduced as much as possible. The ITO glass slide (thickness, 1 mm) is too thick for this purpose. We tried to fabricate freestanding V_2O_5/Pt thin films by the LbL technique using cellulose as a sacrificial layer; however, we obtained only small pieces of freestanding V_2O_5/Pt double film, which is too small to measure its electrochemical properties and is not suitable for its application as a cathode in microbatteries because of its weak mechanical strength. We developed an approach as described in the Experimental Section to design a freestanding V_2O_5 multilayer film to overcome this problem. The multilayer film contained three layers as follows: active V_2O_5 layer, conductive Pt layer, and supporting PVA layer. Figure 6 includes a camera image

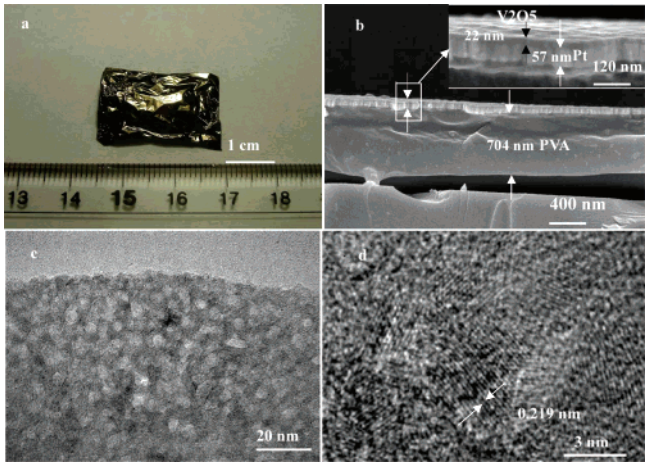

Figure 6. Morphology of V_2O_5/Pt/PVA multilayer film: (a) camera picture, (b) cross-sectional SEM (inset, high-resolution V_2O_5/Pt double layer), (c) TEM, (d) HRTEM.

and SEM and TEM images of a freestanding V_2O_5/Pt/PVA multilayer film. It has a size of 1.9×2.6 cm^2 (Figure 6a) and remains intact and flexible in air. The film surface is smooth without detectable cracks, possessing a morphology similar to that of the V_2O_5 17 nm film on an ITO glass slide. The cross-sectional SEM image of Figure 6b exhibits a uniform, well-distinguished three-layer structure with V_2O_5 as the upper layer, Pt as the middle layer, and PVA as the bottom layer. Their thicknesses are 22, 57, and 704 nm, respectively. The V_2O_5 layer is composed of 4 nm or so of V_2O_5 nanodomains that are closely connected with each other (Figure 6c). An HRTEM image of Figure 6d shows that V_2O_5 nanodomains, as buried in amorphousV_2O_5, have a layered structure with an interplanar spacing of 0.219 nm.

Figure 5A (curve e) shows the specific capacity of the V_2O_5/Pt/PVA multilayer film as a function of the scan rate at two scan ranges. At the scan range of -0.4 to ~ 1.0 V (formation of $Li_{0.93}V_2O_5$), the specific capacity decreases gradually with increasing scan rate. The decrease is 38% upon changing the scan rate from 2 to 400 mV/s. At 250 mV/s, the specific capacity decreases by only 14% after 4000 consecutive cycles (Figure 5B, curve c). Therefore, the V_2O_5/Pt/PVA multilayer film gives excellent performances of fast charge/discharge and very good cycling stability, as in the case of the V_2O_5 17 nm film on ITO. When the potential range was increased to 1.0 to about -1 V vs SCE, the specific capacity of V_2O_5 increases from 133 to 261 mA h per g of V_2O_5 at 2 mV/s (Figure 5A, curve e). The scan-rate dependence is large in this case, and only 53% of the capacity at 2 mV/s is reserved at the very high scan rate of 100 mV/s. The capacity loss after 600 consecutive cycles is 29% (Figure 5B, curve d).

The excellent electrochemical performance of the V_2O_5 ultrathin film is attributed to its special nanostructure. This V_2O_5 nanostructured ultrathin film is composed of 4 nm closely connected V_2O_5 nanodomains and has a thickness of only 17 nm, so Li^+ diffusion distance through both directions of perpendicular and parallel to the substrate are so short that Li^+ ions can easily diffuse into electrochemical active sites from the solvent during intercalation and transport outside into the solvent during extraction. Second, these 4 nm V_2O_5 nanoparticles have a lamellar structure with interlayer distances of 2.19 Å, much larger than the Li^+ size (0.63 Å); such an open structure facilitates free Li^+ accessibility to intercalation active sites in the V_2O_5 ultrathin film. Although the diffusion coefficient of Li^+ in V_2O_5 ($D \approx 1 \times 10^{-12}$ cm^2/s) is much smaller than that in $LiCoO_2$ (5×10^{-9} cm^2/s),[19] the diffusion limit of Li^+ ions was greatly reduced by decreasing the diffusion distance of Li^+ in the V_2O_5 film (e.g., 17 nm). Third, in spite of the small electrical conductivity of V_2O_5 (1×10^{-2} to 1×10^{-3} S/cm), the V_2O_5 ultrathin film can sustain charge/discharge under a large current density because of its low total internal resistance (area specific resistance ASR $= 1 \times 10^{-3}$ to 1×10^{-4} Ω cm^2, thickness of 17 nm), which is much lower than that of bulk $LiCoO_2$ (ASR $= 1 \times 10^{-1}$ to 1×10^{-3} Ω cm^2, thickness of 100 μm).

Park et al.[23] prepared V_2O_5 films by radio frequency magnetron sputtering and investigated the effect of the film thickness on its electrochemical properties. They observed that the films with thicknesses of 1.6 and 3.2 μm showed unstable cycle characteristics and the films with thickness less than 0.8 μm exhibited constant discharge capacity up to the 1000th cycle. Here, we fabricated nanostructured V_2O_5 ultrathin films on conductive layers by spin-coating and found that the film showed fast charge/discharge performance and excellent electrochemical stability. We think that the threshold for thickness of the V_2O_5 film, which limits electrochemical properties, is between 17 and 78 nm in our case.

There have been reported cathode materials, such as $LiCoO_2$, $LiNiO_2$, $LiNi_{1-y}Co_yO_2$, $LiMn_{1-y}Co_yO_2$, iron phosphate, etc.,[19] that can sustain only a low or moderately high charge/discharge rate. Recently, Kang et al.[24] reported a safe, inexpensive cathode material ($Li(Ni_{0.5}Mn_{0.5})O_2$) with a high rate capability. But it is difficult to prepare thin films of cathode from the cathode materials. Nam et al.[25] prepared nanowires of Co_3O_4 by virus-enabled synthesis and assembled them on polyelectrolyte multilayers to form a thin and flexible freestanding cathode film, which can be used as the cathode in microbatteries. We will further decrease the thickness of the supporting film to several tens of nanometers using our newly developed method,[26] replacing the conductive Pt film by other metals (e.g., Au, Ag, Cu, etc.) or directly fabricate a freestanding nanoscale conductive polymer layer to replace the metal/polymer double layers for this purpose. We anticipate that an inexpensive, low toxicity, flexible freestanding thin cathode film with higher total capacity, fast charge/discharge, and the excellent electrochemical stability will be obtained.

(23) Park, Y. J.; Ryu, K. S.; Park, N. G.; Hong, Y. S.; Chang, S. H. *J. Electrochem. Soc.* **2002**, *149*, A597.
(24) Kang, K.; Meng, Y. S.; Breger, J.; Grey, C. P.; Ceder, G. *Science* **2006**, *311*, 977.
(25) Nam, K. T.; Kim, D. W.; Yoo, P. J.; Chiang, C. Y.; Meethong, N.; Hammond, P. T.; Chiang, Y. M.; Belcher, A. M. *Science* **2006**, *312*, 885.
(26) Vendamme, R.; Onoue, S.; Nakao, A.; Kunitake, T. *Nat. Mater.* **2006**, *5*, 494.

Conclusion

In summary, we fabricated uniform V_2O_5 ultrathin films by spin-coating followed by annealing. This V_2O_5 film showed very good electrochemical performance of fast charge/discharge, and excellent electrochemical stability. The excellent electrochemical performance of the V_2O_5 nanostructured ultrathin film is attributed to its short Li^+ diffusion distance and free Li^+ accessibility to intercalation active sites. A flexible and robust freestanding V_2O_5/Pt/PVA multilayer film was fabricated. The freestanding multilayer exhibited excellent electrochemical performance. Such an approach to fabricating a freestanding multilayer film can be applied to fabricate other functional freestanding films for applications such as microsensors.

CM0626233